

# Temperature Compensation Method of Six-Axis Force/Torque Sensor Using Gated Recurrent Unit

(Feb. 2025)

Hyun-Bin Kim, Seokju Lee, Byeong-Il Ham, and Kyung-Soo Kim, *Member, IEEE*,

**Abstract**—This study aims to enhance the accuracy of a six-axis force/torque sensor compared to existing approaches that utilize Multi-Layer Perceptron (MLP) and the Least Square Method. The sensor used in this study is based on a photo-coupler and operates with infrared light, making it susceptible to dark current effects, which cause drift due to temperature variations. Additionally, the sensor is compact and lightweight (45g), resulting in a low thermal capacity. Consequently, even small amounts of heat can induce rapid temperature changes, affecting the sensor's performance in real time. To address these challenges, this study compares the conventional MLP approach with the proposed Gated Recurrent Unit (GRU)-based method. Experimental results demonstrate that the GRU approach, leveraging sequential data, achieves superior performance.

**Index Terms**—Force measurement, Torque measurement, Measurement errors

## I. INTRODUCTION

RECENTLY, various types of robots, including collaborative robots, legged robots, and mobile robots, have been actively researched [1]–[5]. Force/Torque (F/T) sensors are widely used in these robots [6], [7], with strain gauge-based sensors being the most common. In addition to strain gauges, capacitance-based F/T sensors are also utilized [8]–[10], as they enable precise measurement of forces and torques.

These sensors serve various purposes in different robotic applications. In collaborative robots, they are employed for admittance control [11], grasping objects, and determining the position of the end-effector. In legged robots, particularly bipedal robots, F/T sensors are frequently used to measure ground reaction forces, which play a crucial role in walking control by enabling the calculation of Zero Moment Point (ZMP) [12] or Capture Point [13]. In mobile robots, these sensors are often attached to robotic arms for object manipulation. In quadrupedal robots, pneumatic pressure sensors are commonly used to detect contact [14].

Manuscript created September, 2024; This work was developed by the MSC (Mechatronics, Systems and Control) lab in the KAIST (Korea Advanced Institute of Science and Technology) which is in the Daehak-Ro 291, Daejeon, South Korea (e-mail: youfree22@kaist.ac.kr; dltjrwn0322@kaist.ac.kr; byongil\_ham@kaist.ac.kr; kyungsookim@kaist.ac.kr). (Corresponding author: Kyung-Soo Kim).

However, F/T sensors, particularly those based on strain gauges, are susceptible to drift or offset due to thermal expansion caused by temperature variations. Various methods have been proposed to address this issue, which can be broadly categorized into two approaches. The first is model-based methods, while the second involves the use of artificial neural networks or support vector machines.

Model-based methods primarily utilize linear approaches, incorporating a calibration matrix and a function of temperature as follows:

$$f = Cr + o + C_t t \quad (1)$$

[15] where  $C$  represents the calibration matrix,  $o$  denotes the offset,  $C_t$  refers to the temperature calibration coefficients, and  $t$  is the temperature value. This method employs the Least Square Method, and similar approaches have been used in [15]–[17]. In fiber grating-based methods, an analytical model-based approach has been implemented using heat transfer models [18] or the Least Square Method. Additionally, for piezoresistive sensors [19], model-based methods incorporating the characteristics of the Wheatstone bridge have been applied. Linear models have also been utilized in some studies.

Research employing Support Vector Machines (SVM) and Artificial Neural Networks (ANN) [20] for thermal compensation includes various approaches. One such approach involves using a Multi-Layer Perceptron (MLP) with Radial Basis Functions (RBF) [21]. Subsequent studies have optimized RBF networks using particle swarm optimization and applied the Least Square Support Vector Machine (LSSVM) [22]. Other approaches include employing MLP with Leaky ReLU activation functions or optimizing using the Adaptive Genetic Algorithm-Back Propagation (AGA-BP) method [26]. Moreover, additional studies have implemented thermal compensation using SVM, K-nearest neighbors (KNN), Random Forest, and Decision Trees [23].

However, in most of these studies, modeling is often simplified, assuming no axis interference or that the sensor weight is in the kilogram range, allowing thermal compensation to reach a steady state. Linear models introduce significant compensation errors when approximating nonlinear drift as a linear model. Furthermore, for heavy sensors that maintain

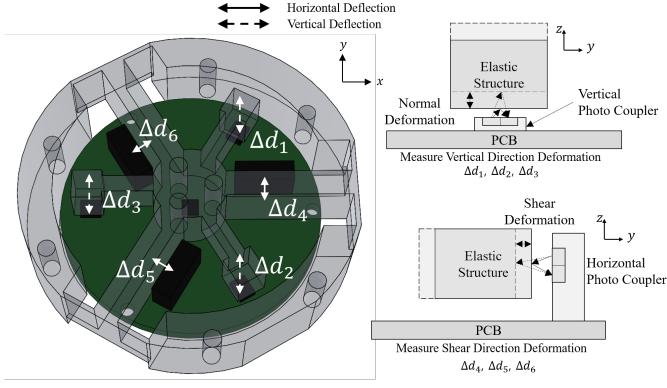


Fig. 1. A novel six-axis force/torque sensor using photo-couplers: Distance between Vertical Photo-coupler and Reflective Surface of Elastic Structure  $\Delta d_1, \Delta d_3, \Delta d_5$ , Distance between horizontal Photo-coupler and Reflective Surface of Elastic Structure  $\Delta d_2, \Delta d_4, \Delta d_6$

a steady-state temperature, the use of MLP does not lead to significant errors.

This study aims to address temperature-induced drift in a small sensor (diameter 40 mm, 45 g weight) [24], [25] that experiences rapid temperature variations due to low thermal mass. The key contributions of this work are as follows. To compensate for sensor drift, time sequence data is utilized for training, and a Gated Recurrent Unit (GRU) [27], a type of Recurrent Neural Network (RNN) commonly used in natural language models, is employed. Experiments compare the proposed approach with the Least Square Method and MLP-based training, demonstrating that the proposed method exhibits lower errors and superior performance in scenarios where temperature continuously varies over time.

This approach has the potential to be applied to various sensors, particularly in cases where nonlinearities arise due to temperature variations.

## II. A NOVEL SIX-AXIS FORCE/TORQUE SENSOR USING PHOTO-COUPPLERS

A novel six-axis force/torque sensor is presented in Fig. 1. The measurement principle of this sensor is based on reflective photo-couplers. The sensor incorporates a total of six photo-couplers: three oriented vertically, primarily measuring the vertical force component (the force along the  $z$ -axis) and the moments about the  $x$ - and  $y$ -axes. The remaining three photo-couplers are oriented horizontally and are mainly used to measure the horizontal force components (the forces along the  $x$ - and  $y$ -axes) and the moment about the  $z$ -axis.

The sensor has a compact diameter of 40 mm and a lightweight design, weighing approximately 45 g. It integrates an Analog to Digital Converter(ADC), an Micro-Controller Unit(MCU), and a temperature sensor, enabling direct communication of the measured values via the CAN protocol. The measurement range is approximately 600 N for the forces along the  $x$ - and  $y$ -axes, 2000 N for the force along the  $z$ -axis, 14 N·m for the moments about the  $x$ - and  $y$ -axes, and 20 N·m for the moment about the  $z$ -axis.

A TMP117 IC temperature sensor, which communicates via I2C, is mounted at the center of the printed circuit board. This sensor features an accuracy of  $0.08^\circ\text{C}$  and a resolution of  $7.8125 \text{ m}^\circ\text{C}$ . In this study, it was utilized for temperature measurement and incorporated into the compensation algorithm.

Despite its small diameter and wide measurement range, the sensor achieves enhanced sensitivity through optimization via modeling and global search methods, providing a resolution of approximately 14 bits. The sensor is specifically designed for integration into the feet of legged robots, ensuring robustness against impact forces.

## III. PROPOSED METHOD AND LEARNING OF NETWORK

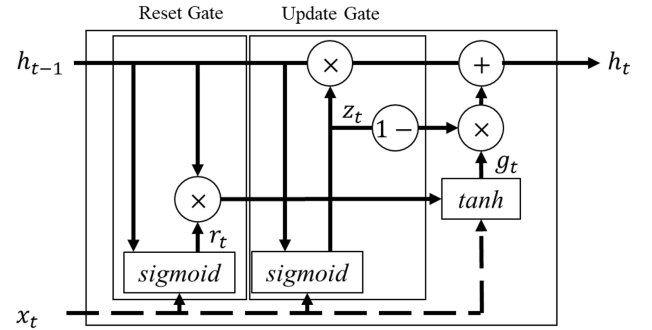


Fig. 2. Structure of Gated Recurrent Unit

In conventional methods, the Multi-Layer Perceptron (MLP) has been the most widely used approach, as shown in Fig. 2(a). MLP is a fundamental artificial neural network architecture that is particularly effective for training models with high nonlinearity. It consists of an input layer, multiple hidden layers, and an output layer. The hidden layers utilize non-linear activation functions such as ReLU or Tanh to optimize parameters.

Additionally, the Temporal Convolutional Network (TCN) [28], as illustrated in Fig. 2(b), processes sequence inputs through convolutional operations, making it highly effective in capturing features from sequential data. TCN is known for its capability to extract meaningful features from short-term time series data.

The proposed method employs the Gated Recurrent Unit (GRU), a type of Recurrent Neural Network (RNN) commonly used in language models. GRU provides similar performance to Long Short-Term Memory (LSTM) networks [29] but with fewer parameters, making it a more efficient choice for temperature compensation. The structure of GRU is depicted in Fig. 2(c), where the time sequence input  $x_t$  is processed using reset and update gates along with the previous output to generate the final output.

$$\begin{aligned} r_t &= \sigma(W_{xr}x_t + W_{hr}h_{t-1}) \\ z_t &= \sigma(W_{xz}x_t + W_{hz}h_{t-1}) \\ g_t &= \tanh(W_{hg}(r_t \otimes h_{t-1}) + W_{xg}x_t) \\ h_t &= (1 - z_t) \otimes g_t + z_t \otimes h_{t-1} \end{aligned} \quad (2)$$

The reset gate determines how much of the previous state information should be retained in the current state. When the reset gate value is close to 0, the previous state information is forgotten, whereas when it is close to 1, the previous state information is preserved. The update gate in Fig. 2(c) plays a crucial role in balancing the contribution of previous state information and newly acquired information.

The update gate value  $z_t$  is a real number between 0 and 1. When  $z_t$  is close to 1, the previous state information is prioritized, whereas when it is close to 0, the new information is emphasized. If  $z_t$  is equal to 1, the signal passing through the operation  $1 - z_t$  becomes zero, thereby disabling the input gate. Conversely, when  $z_t$  is 0, the forget gate does not operate, and only the input gate is activated.

Through this mechanism, the GRU effectively balances the previous and current state information. Eq. 2 presents the mathematical formulation of the gate operations within the GRU.

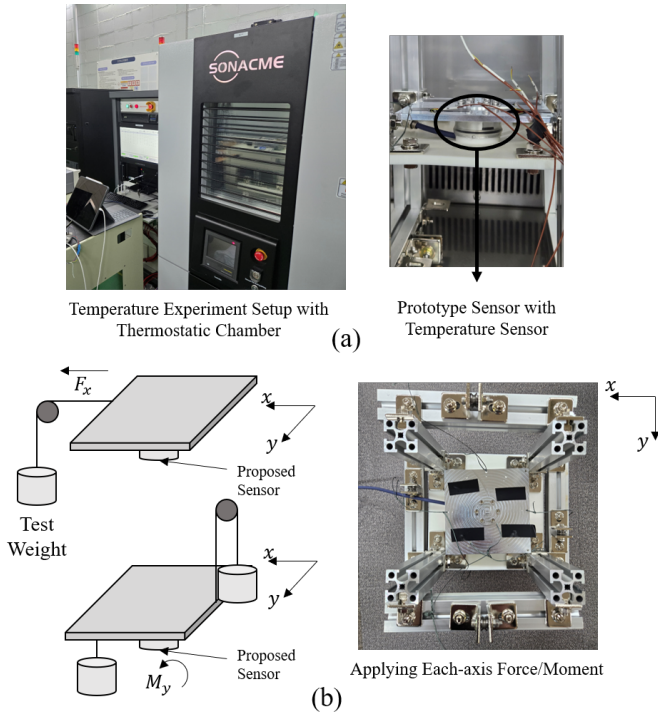


Fig. 3. Temperature Data Acquisition Experiment:(a) Temperature Experiment Setup with Thermostatic Chamber (b) Equipment of Applying Static Force/Moment

To evaluate the learning performance of conventional methods such as MLP, TCN, and GRU, an initial data acquisition experiment was conducted. The data was obtained using a thermostatic chamber, as illustrated in Fig. 3. To assess the impact of forces along each axis on temperature compensation—specifically, the relationship between the sensor gain and temperature—the sensor was subjected to applied forces. Additionally, forces along each axis were measured using a test weight. The temperature was varied between  $-20^{\circ}\text{C}$  and  $60^{\circ}\text{C}$  during the experiment.

The data corresponding to temperature variations were

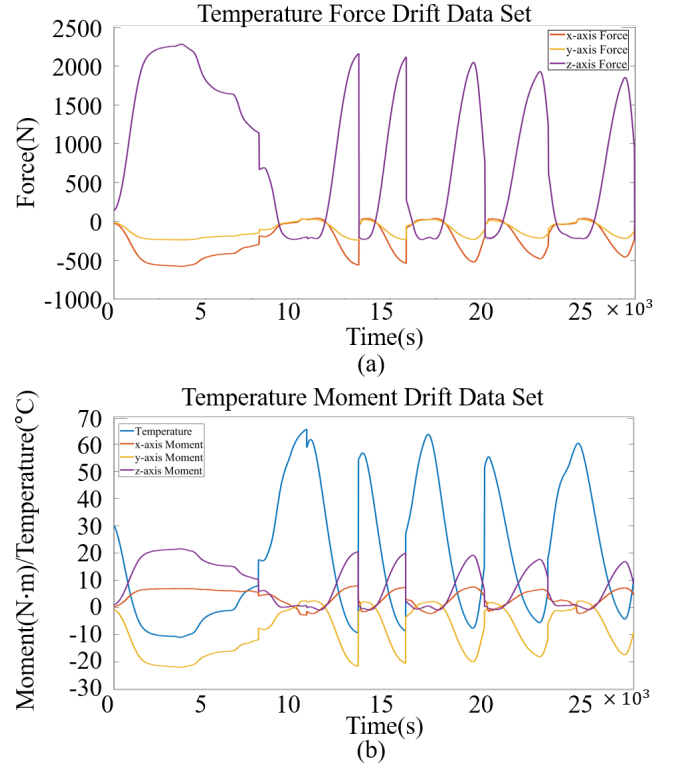


Fig. 4. Temperature Drift Data Set: (a) Force (b) Moment

measured by repeatedly cycling the temperature from  $-20^{\circ}\text{C}$  to  $60^{\circ}\text{C}$  under normal conditions. The results are presented in Fig.4. As shown in Fig.4(b), the temperature was varied accordingly. The force drift for each output is depicted in Fig.4(a), while the moment drift is illustrated in Fig.4(b).

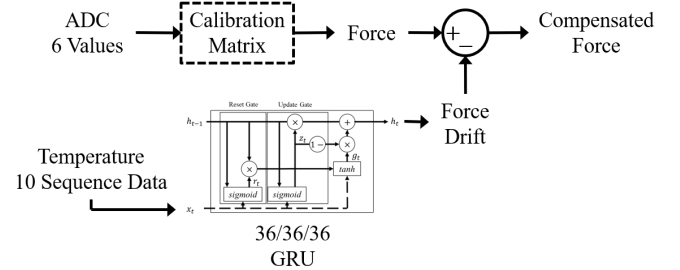


Fig. 5. Diagram of Temperature Compensation Algorithm: Calculate Force Value from 6 ADC inputs and Calibration Matrix, Calculate Force Drift from 10 Sequence Temperature Sensor Data.

Fig.5 presents a diagram illustrating the temperature compensation method for the novel six-axis force/torque sensor. The process begins with the acquisition of six ADC values from the photo-couplers, which are then processed through a calibration matrix to compute the force. Subsequently, a learning algorithm, trained using a sequence of 10 temperature data points, predicts the force/moment drift. The compensated force is then calculated based on this prediction. Additionally, the Gated Recurrent Unit (GRU) in Fig.5 can be replaced with

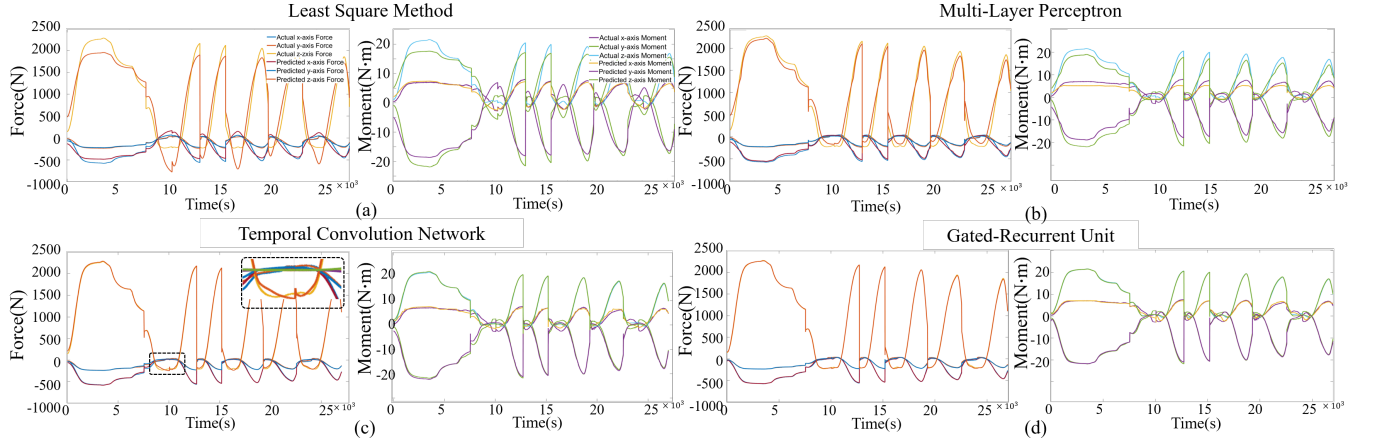


Fig. 6. Comparison of learning performance across different methods (Least Square Method, MLP, TCN, GRU): (a) Fitting results using the Least Square Method (b) Fitting results using the Multi-Layer Perceptron (MLP) (c) Fitting results using the Temporal Convolutional Network (TCN) (d) Fitting results using the Gated Recurrent Unit (GRU)

other network architectures, such as a Multi-Layer Perceptron (MLP) or a Temporal Convolutional Network (TCN), allowing for the application of different networks in the same framework.

A comparison of the four learning methods is presented in Fig. 6. The Least Square Method, a Multi-Layer Perceptron (MLP) with three layers and 36 nodes per layer, a Temporal Convolutional Network (TCN), and a Gated Recurrent Unit (GRU) were evaluated. In this study, the input consists of temperature data, including both single data points and sequences, while the output represents the estimated force drift. The Adam optimizer was used for training, with a maximum of 2000 epochs. The learning rate was set to 0.001, the batch size was 128, and the mean squared error (MSE) was employed as the loss function.

The Least Square Method exhibited significant errors in temperature compensation due to its inability to handle strong nonlinearity. Similarly, the MLP struggled to achieve proper fitting as temperature variations occurred over time. In contrast, both the TCN and GRU demonstrated significantly better fitting performance. However, while the TCN effectively captured short-term temporal dependencies, temperature variations occur over extended periods, making the GRU more suitable for this task. As a result, the GRU achieved the most accurate fitting among the evaluated methods.

TABLE I  
RMSE AFTER CONVERGENCE FOR EACH METHOD

Method	LSM	MLP	TCN	GRU
RMSE	~500	~100	~40	~5

As shown in Table I, the RMSE for the Least Square Method (LSM) is close to 500, indicating a large error. The MLP also exhibits a relatively high RMSE of approximately 100. In contrast, the TCN achieves an RMSE of 40, while the GRU achieves an RMSE below 5. This demonstrates that the GRU achieves the best convergence and fitting performance, with an RMSE that is nearly 1/100th of that of the LSM.

#### IV. ALGORITHM VALIDATION EXPERIMENT

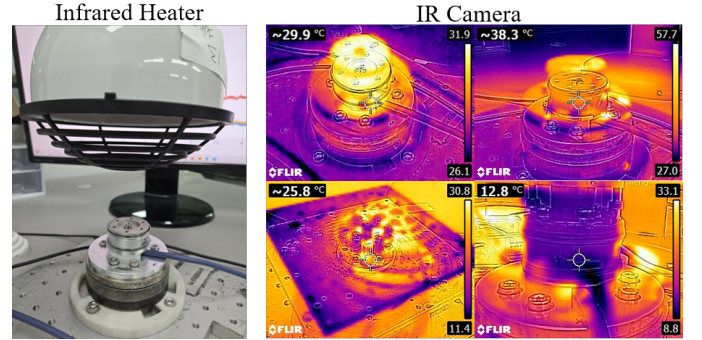


Fig. 7. Temperature Compensation Experiment using Infrared Heater and Ice for Verification

An experiment was conducted to verify whether the fitted function operates effectively in real-world conditions rather than in the controlled environment of a thermostatic chamber. The experiment utilized an infrared heater, as employed in previous study [17], to increase the temperature, while an ice pack was used to decrease it.

The experiment consisted of two parts: one for increasing the temperature and another for decreasing it. In the heating experiment, the temperature was increased by 10°C over approximately 200 seconds, while in the cooling experiment, the temperature was decreased at a rate of 5°C over approximately 300 seconds.

The experimental results are presented in Fig. 8. The comparison includes cases without compensation, with compensation using an MLP, with an MLP trained using a sequence of 10 temperature data points, and with a Gated Recurrent Unit (GRU). The MLP trained with 10 sequential temperature data points showed improved learning performance, achieving an RMSE of approximately 40, similar to the TCN, and outperforming the conventional MLP.



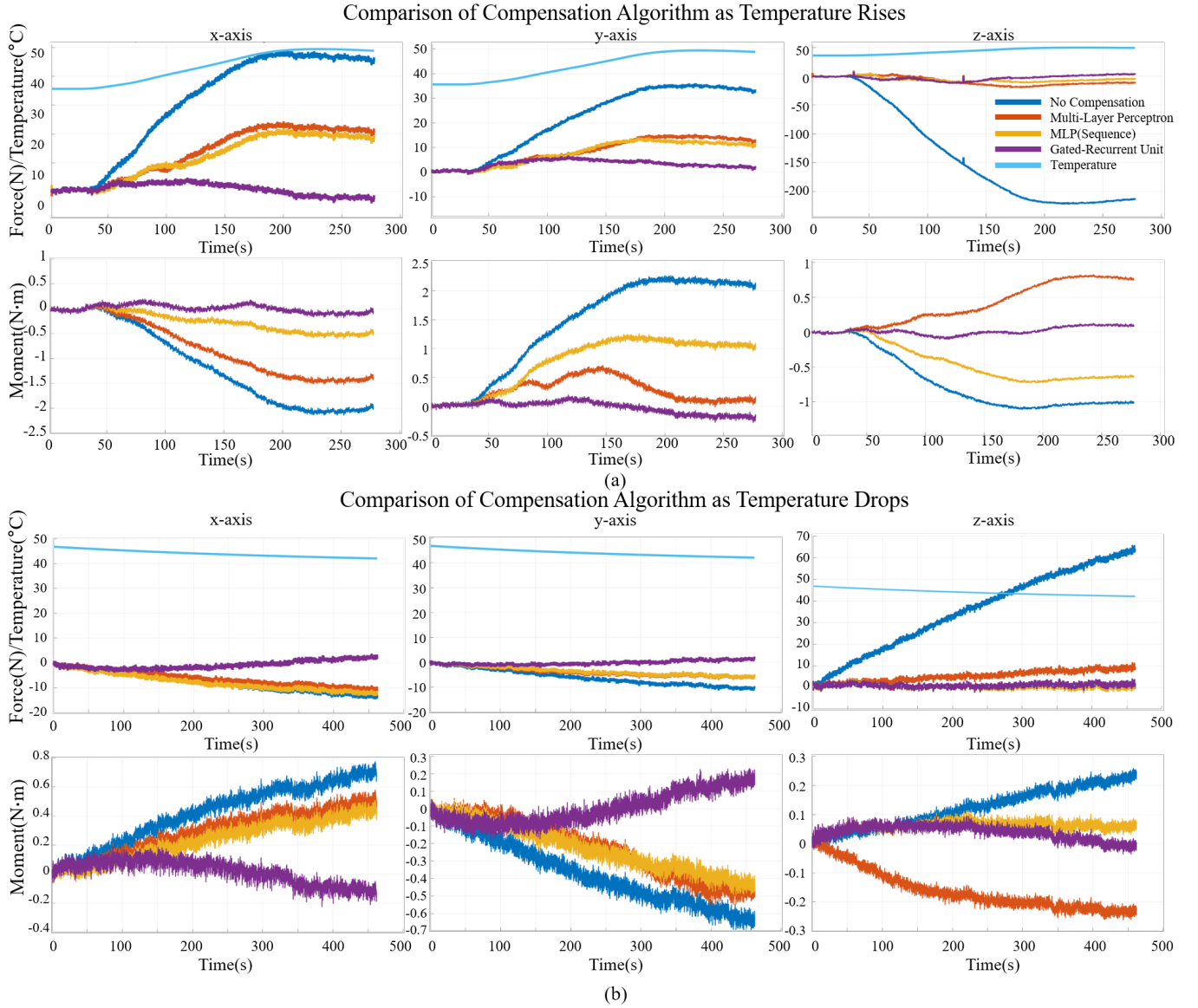


Fig. 8. Comparison of Compensation Algorithm as Temperature Changes: (a) Experiment Results at Temperature Rises (b) Experiment Results at Temperature Drops

Fig.8(a) presents the experimental results when using the temperature compensation method described in Fig.5 during temperature increase, with no external force applied to any axis. The results show that the compensation method using the GRU effectively eliminates drift across all axes.

In the z-axis force, both the GRU and the MLP trained with sequential temperature data exhibit similar performance. However, the MLP demonstrates a tendency to learn nonlinearities better than the GRU. This is likely due to the fact that the vertical photo-coupler, responsible for the z-axis measurement in the novel force/torque sensor, is positioned farther from the reflective surface compared to the horizontal photo-couplers. Consequently, it is more susceptible to ambient dark current effects, resulting in greater nonlinearity.

Fig. 8(b) presents the experimental results for temperature

compensation during temperature decrease, again with no external force applied to any axis. The results confirm that the GRU exhibits the least drift, providing significantly better compensation compared to the MLP.

TABLE II  
RMS ERROR COMPARISON BETWEEN COMPENSATION METHOD WHEN TEMPERATURE DECREASES

RMSE	$F_x(N)$	$F_y(N)$	$F_z(N)$	$M_x(N\cdot m)$	$M_y(N\cdot m)$	$M_z(N\cdot m)$
No compensation	8.6585	6.8711	40.009	0.4673	0.4128	0.1409
MLP	6.8087	4.2006	5.8157	0.3293	0.2819	0.1750
MLP(Sequence)	8.3733	3.9628	0.9649	0.2717	0.2636	0.0631
GRU	1.7778	0.8667	1.2555	0.0824	0.0903	0.0454

Table II presents the RMSE values corresponding to the results in Fig. 8(a). The GRU demonstrated consistently superior performance across all axes. Although there was a

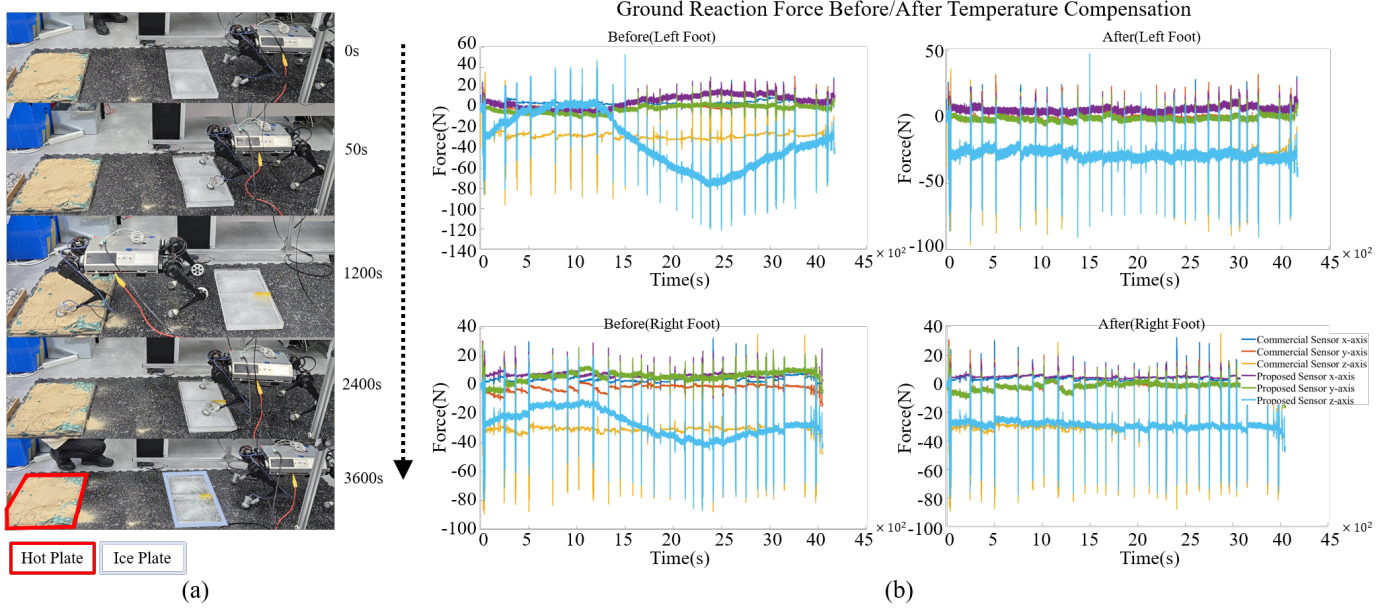


Fig. 9. Temperature Compensation Experiment in Quadruped Application: (a) Walking Experiment Ice Plate and Hot Plate (b) Graph of Ground Reaction Force Before/ After Temperature Compensation

TABLE III

RMS ERROR COMPARISON BETWEEN COMPENSATION METHOD WHEN TEMPERATURE INCREASES

RMSE	$F_x(N)$	$F_y(N)$	$F_z(N)$	$M_x(N\cdot m)$	$M_y(N\cdot m)$	$M_z(N\cdot m)$
No compensation	35.381	25.317	159.82	1.3810	1.6356	0.8197
MLP	16.003	10.039	11.315	0.9624	0.3397	0.4881
MLP(Sequence)	14.086	9.1935	7.0742	0.3259	0.8862	0.5026
GRU	2.1518	3.7264	5.1868	0.0749	0.1031	0.0557

slight difference of approximately 0.3 N in the z-axis force compared to the MLP trained with sequential data, the overall performance of the GRU was approximately four times better.

Table III summarizes the RMSE values for the results shown in Fig. 8(b). In this case, the GRU achieved the best performance across all axes. Notably, in the z-axis force, the RMSE was reduced from 160 N without compensation to approximately 5 N. Similarly, in the x-axis force, the drift was reduced from 35 N to approximately 2 N. This corresponds to a maximum full-scale error of approximately 0.2%.

In the previous experiments, tests were conducted using the sensor alone. However, to further validate its real-world applicability through comparative analysis, an experiment was performed by mounting both a commercial sensor and the novel force/torque sensor on the foot of a quadruped robot using GRU-based temperature compensation algorithm. This setup allowed for direct comparison and evaluation in practical conditions.

For the commercial sensor, the RFT-40 model from Robotus was used. This capacitive-type sensor was selected due to its minimal sensitivity to temperature variations. The experiment setup is illustrated in Fig. 9.

Fig. 9(a) depicts the experimental procedure, where the robot initially stepped onto a  $-20^{\circ}\text{C}$  ice plate. After 20 minutes,

it moved onto a  $70^{\circ}\text{C}$  hot plate, heated using hand warmers, and remained there for another 20 minutes. The robot then stepped back onto a new ice plate at  $-20^{\circ}\text{C}$  for an additional 20 minutes, replicating realistic temperature variations in a controlled manner.

Fig. 9(b) presents the measured ground reaction forces (GRFs) of the left and right feet during the experiment. The graph on the left shows the GRF before applying temperature compensation, while the graph on the right illustrates the results after compensation.

TABLE IV

RMS ERROR COMPARISON BETWEEN BEFORE AND AFTER COMPENSATION DURING WALKING EXPERIMENT

RMSE	$F_x(N)$	$F_y(N)$	$F_z(N)$
Left Foot(Before)	6.280	3.084	25.502
Left Foot(After)	1.224	2.145	2.714
Right Foot(Before)	3.399	8.274	9.864
Right Foot(After)	1.369	1.136	2.831

As a result of the experiment, the RMSE values were calculated as shown in Table IV. For the sensor on the left foot, the RMSE of the z-axis force was 26 N without temperature compensation. However, after applying compensation, it was reduced to 2.7 N, nearly a tenfold improvement. A similar trend was observed for the right foot, confirming that the temperature compensation method was effectively applied.

## V. CONCLUSION

This study proposed a temperature compensation algorithm for a novel six-axis force/torque sensor using a Gated Recurrent Unit (GRU)-based learning approach. Unlike conventional methods such as the Least Square Method (LSM) and

Multi-Layer Perceptron (MLP), which struggle with nonlinear temperature-induced drift, the GRU effectively captured temporal dependencies, enabling robust compensation even under continuous temperature variations.

To validate the proposed method, multiple experiments were conducted. Initially, controlled experiments in a thermostatic chamber demonstrated that the GRU significantly outperformed other approaches, achieving an RMSE nearly 100 times lower than LSM and approximately four times lower than MLP. Further validation was performed in real-world conditions using an infrared heater and an ice pack, confirming the effectiveness of the GRU-based compensation compared to MLP and Temporal Convolutional Networks (TCN). Additionally, an application experiment was conducted by integrating the sensor into the foot of a quadruped robot alongside a commercial capacitive force sensor. The results showed that temperature drift, which initially reached 26 N in the z-axis, was reduced to 2.7 N after compensation, demonstrating nearly a tenfold improvement.

These findings indicate that the proposed GRU-based temperature compensation method effectively mitigates the impact of temperature-induced drift, even in small and lightweight force/torque sensors that are highly susceptible to thermal fluctuations. The proposed approach has the potential to be applied to various sensors requiring robust compensation against nonlinear temperature effects, making it particularly beneficial for applications in legged robots and other robotic systems operating in dynamic environments. Future research could explore further optimization of network architectures and extend the method to compensate for additional environmental factors affecting sensor performance.

## REFERENCES

- [1] J. Di Carlo, P. M. Wensing, B. Katz, G. Bledt, and S. Kim, "Dynamic locomotion in the mit cheetah 3 through convex model-predictive control," in *2018 IEEE/RSJ International Conference on Intelligent Robots and Systems (IROS)*, 2018, pp. 1–9.
- [2] M. Hutter *et al.*, "Anymal-a highly mobile and dynamic quadrupedal robot," in *2016 IEEE/RSJ International Conference on Intelligent Robots and Systems (IROS)*, 2016, pp. 38–44.
- [3] J. Kang, H.-B. Kim, K. H. Choi, and K.-S. Kim, "External force estimation of legged robots via a factor graph framework with a disturbance observer," in *2023 IEEE International Conference on Robotics and Automation (ICRA)*, 2023, pp. 12 120–12 126.
- [4] J. Kang, H.-B. Kim, B.-I. Ham, and K.-S. Kim, "External force adaptive control in legged robots through footstep optimization and disturbance feedback," *IEEE Access*, 2024.
- [5] J. Kang, H. Kim, and K.-S. Kim, "View: Visual-inertial external wrench estimator for legged robots," *IEEE Robotics and Automation Letters*, vol. 8, no. 12, pp. 8366–8373, 2023.
- [6] Y. Li *et al.*, "Impedance learning-based adaptive force tracking for robot on unknown terrains," *IEEE Transactions on Robotics*, 2025.
- [7] G. Valsecchi, R. Grandia, and M. Hutter, "Quadrupedal locomotion on uneven terrain with sensorized feet," *IEEE Robotics and Automation Letters*, vol. 5, no. 2, pp. 1548–1555, 2020.
- [8] U. Kim *et al.*, "A novel six-axis force/torque sensor for robotic applications," *IEEE/ASME Transactions on Mechatronics*, vol. 22, no. 3, pp. 1381–1391, 2016.
- [9] U. Kim *et al.*, "Sensorized surgical forceps for robotic-assisted minimally invasive surgery," *IEEE Transactions on Industrial Electronics*, vol. 65, no. 12, pp. 9604–9613, 2018.
- [10] M. Pu *et al.*, "Modeling for elastomer displacement analysis of capacitive six-axis force/torque sensor," *IEEE Sensors Journal*, vol. 22, no. 2, pp. 1356–1365, 2021.
- [11] J. Chen *et al.*, "Adaptive-constrained admittance control for physical human–robot interaction," *Transactions of the Institute of Measurement and Control*, 2025.
- [12] S. Kajita *et al.*, "Biped walking pattern generation by using preview control of zero-moment point," in *2003 IEEE International Conference on Robotics and Automation*, 2003, vol. 2, pp. 1620–1626.
- [13] J. Pratt *et al.*, "Capture point: A step toward humanoid push recovery," in *2006 6th IEEE-RAS International Conference on Humanoid Robots*, 2006, pp. 200–207.
- [14] "Unitree robotics," Available: <https://www.unitree.com/>, Accessed: 2025-01-21.
- [15] J. Scott and E. T. Enikov, "Novel temperature compensation technique for force-sensing piezoresistive devices," *Journal of Micromechanics and Microengineering*, vol. 21, no. 11, p. 115017, 2011.
- [16] F. J. A. Chavez *et al.*, "Model-based in situ calibration with temperature compensation of 6-axis force torque sensors," in *2019 International Conference on Robotics and Automation (ICRA)*, 2019, pp. 5397–5403.
- [17] P. Billeschou *et al.*, "A low-cost, compact, sealed, three-axis force/torque sensor for walking robots," *IEEE Sensors Journal*, vol. 21, no. 7, pp. 8916–8926, 2021.
- [18] H.-P. Wang *et al.*, "Improved temperature compensation of fiber Bragg grating-based sensors applied to structures under different loading conditions," *Optical Fiber Technology*, vol. 63, p. 102506, 2021.
- [19] D. F. Wang *et al.*, "A temperature compensation methodology for piezoelectric-based sensor devices," *Applied Physics Letters*, vol. 111, no. 8, 2017.
- [20] N. Kazemi *et al.*, "A temperature-compensated high-resolution microwave sensor using artificial neural networks," *IEEE Microwave and Wireless Components Letters*, vol. 30, no. 9, pp. 919–922, 2020.
- [21] Y. Sun *et al.*, "Temperature compensation for six-dimension force/torque sensor based on radial basis function neural network," in *2014 IEEE International Conference on Information and Automation (ICIA)*, 2014, pp. 789–794.
- [22] Y. Sun *et al.*, "Temperature compensation for a six-axis force/torque sensor based on the particle swarm optimization least square support vector machine for space manipulator," *IEEE Sensors Journal*, vol. 16, no. 3, pp. 798–805, 2015.
- [23] N. Kazemi *et al.*, "Comparative analysis of machine learning techniques for temperature compensation in microwave sensors," *IEEE Transactions on Microwave Theory and Techniques*, vol. 69, no. 9, pp. 4223–4236, 2021.
- [24] H.-B. Kim *et al.*, "Parameter optimization of optical six-axis force/torque sensor for legged robots," *arXiv preprint arXiv:2502.07196*, 2025.
- [25] H.-B. Kim *et al.*, "A compact six-axis force/torque sensor using photo-couplers for impact robustness," *Review of Scientific Instruments*, vol. 95, no. 4, 2024.
- [26] Z. Han *et al.*, "Temperature drift modeling and compensation of capacitive accelerometer based on AGA-BP neural network," *Measurement*, vol. 164, p. 108019, 2020.
- [27] K. Cho *et al.*, "Learning phrase representations using RNN encoder-decoder for statistical machine translation," *arXiv preprint arXiv:1406.1078*, 2014.
- [28] S. Bai, J. Z. Kolter, and V. Koltun, "An empirical evaluation of generic convolutional and recurrent networks for sequence modeling," *arXiv preprint arXiv:1803.01271*, 2018.
- [29] S. Hochreiter and J. Schmidhuber, "Long short-term memory," *Neural Computation*, vol. 9, no. 8, pp. 1735–1780, 1997.



**Hyun-Bin Kim** received the B.S., M.S. and Ph.D. degrees in mechanical engineering from Korea Advanced Institute of Science and Technology (KAIST), Daejeon, Republic of Korea, in 2020, 2022 and 2025 respectively. He is currently working as the post-doctor researcher in KAIST. His current research interests include force/torque sensors, legged robot control, robot design and mechatronics system.



**Seokju Lee** received the B.S. degree in electrical engineering from Ulsan National Institute of Science and Technology (UNIST), Ulsan, Republic of Korea, in 2023, and the M.S. degree in mechanical engineering from Korea Advanced Institute of Science and Technology (KAIST), Daejeon, Republic of Korea, in 2025. He is currently working toward the Ph.D. degree with the Department of Mechanical Engineering, KAIST. His research interests include legged robots, state estimation, and reinforcement learning.



**Byeong-Il Ham** received the B.S. degree in school of robotics from University of Kwang-woon, Seoul, and the M.S. degree in robotics program from Korea Advanced Institute of Science and Technology (KAIST), Daejeon, Republic of Korea, in 2022 and 2024, respectively. He is in Doctor Program in KAIST, Daejeon, Korea, from 2024. His current research interests include legged system, optimal control and motion planning.



**Kyung-Soo Kim** (Fellow, IEEE) received the B.S., M.S., and Ph.D. degrees in mechanical engineering from Korea Advanced Institute of Science and Technology (KAIST), Daejeon, Republic of Korea, in 1993, 1995, and 1999, respectively. He was a Chief Researcher with LG Electronics Inc., from 1999 to 2003, and the DVD Group Manager of STMicroelectronics Company Ltd., from 2003 to 2005. In 2005, he joined the Department of Mechanical Engineering, Korea Polytechnic University, Siheung, Republic of Korea, as a Faculty Member. Since 2007, he has been with the Department of Mechanical Engineering, KAIST. His research interests include control theory, electric vehicles, and autonomous vehicles. He serves as an Associate Editor for the Automatica and the Journal of Mechanical Science and Technology.